COMPUTER GRAPHICS AND IMAGE PROCESSING 20, 229–243 (1982)

# Detection of Osteogenesis Imperfecta by Automated Texture Analysis[1]

DEMETRI TERZOPOULOS AND STEVEN W. ZUCKER

*Computer Vision and Graphics Laboratory, Department of Electrical Engineering, McGill University, Montreal, Quebec, Canada*

Received August 8, 1980; revised November 17, 1981

An automated system for detecting Osteogenesis Imperfecta (OI), an inheritable disorder of human connective tissue, is described. The approach is one of texture analysis, founded on standard statistical recognition of co-occurrence-based texture descriptors. Our contribution is to show that texture descriptors derived from gray-level co-occurrence matrices can be used in conjunction with descriptors derived from generalized co-occurrence matrices of local image features to increase performance. In fact, for the OI problem, our system demonstrates a level of performance which is significantly better than that of medical specialists.

## 1. INTRODUCTION

Images are certainly one of the most common forms of data representation in biology and medicine. When they represent experimental results, isolation and quantification of the information within them is often paramount to a successful analysis. When they represent the results of diagnostic tests, questions of enhancement, consistency, and reliability become important. Computer-based image processing techniques are currently making a substantial contribution to both of these areas. The research described in this paper is a new biomedical application of a particular class of these techniques, texture analysis, to the diagnosis of Osteogenesis Imperfecta (OI), an inheritable disease of human connective tissue.

Over the past two decades, researchers interested in texture analysis by computer have proposed a number of techniques and models for texture [4]. Most of these approaches measure statistical properties of texture. A very useful and popular statistical approach involves the characterization of textures by what are, essentially, two-dimensional distributions of occurrences of pairs of image pixel intensities, or attributes of more complex local image features. The former are often termed gray-level co-occurrence matrices (GLCM) [5] and the latter are called generalized co-occurrence matrices (GCM) [2]. Weszka, *et al.* [11] have shown empirically that co-occurrence matrices are one of the most powerful representations for texture known to date.

Psychophysiological justification for the use of co-occurrence matrices in characterizing textures can be found among the literature on human texture perception. In an early study [6], Julesz discovered what appeared at the time to be a surprisingly universal phenomenon of human, noncognitive texture perception: that

[1]This research was supported by MRC Grant MA-6154. We would like to thank the members of the deBelle Laboratory for Biochemical Genetics of the McGill University—Montreal Children's Hospital Research Institute, particularly Drs. H. Goldman, R. Gold, and G. Lancaster, for both supplying us with the OI culture data and for serving as a panel of expert diagnosticians, and G. Brighten for conducting the expert classification experiments.



0146-664X/82/110229-15$02.00/0
Copyright © 1982 by Academic Press, Inc.
All rights of reproduction in any form reserved.

differences in second-order statistics of image intensities are sufficient for spontaneous discrimination of textures. In later studies (see, e.g., [1]), however, he found counterexamples to this conjecture; that is, he found discriminable textures with equal second-order intensity statistics. Julesz argued that these counterexamples may be explained by assuming that low-level feature detectors act on the retinal image to extract local features which are more complex than the raw intensities. Since GLCMs are measurements of second-order intensity statistics, and GCMs are measurements of second-order statistics of local features, their utility in analyzing textures is supported by Julesz's conjectures about texture vision. Additional support for the use of local image features for texture analysis is provided by Marr's computational theory of low-level vision [8]. The significance of the above ideas in the application of co-occurrence matrices to texture analysis is explored more fully in [10].

Following a brief discussion of the nature of OI and a formulation of the GLCM and the GCM, we describe a system which uses texture descriptors, derived from both types of matrices, to distinguish between images of normal and OI cell cultures. We show that our system attains a performance which is significantly (about 20%) better than that exhibited by a group of six medical specialists attempting to discriminate the same images by visual inspection.

## 2. OSTEOGENESIS IMPERFECTA

Osteogenesis Imperfecta is a highly prevalent, genetically determined disease [9]. It has an extremely broad range of clinical expressivity, usually involving bone tissue; although skin, ligaments, tendons, fascia, sclera, and the inner ear are often implicated. Common manifestations are brittle bones susceptable to multiple fractures, as well as deafness, blue sclera, thin skin, slow healing of wounds, loose joints, and hernia. The disease is most commonly inherited as a Mendelian autosomal dominant. Current views are that OI is characteristic of a defect in the maturation or synthesis of one of the structural proteins, probably collagen.

Researchers at the Montreal Children's Hospital have discovered that OI skin fibroblasts, cultured in vitro, exhibit a morphological defect when compared with normal cells. Specifically, "normal cells in log phase have an elongated spindle shape, whereas OI cells at the same stage of growth in log phase are tesselated and irregular in shape. The difference between OI and normal cells is exaggerated in the stationary phase of culture. The shape of normal fibroblasts allows them to intercalate with each other in a regular or "smooth" pattern. On the other hand, the OI fibroblasts, because of their irregular shapes, present a "rough" appearance" [7, p. 85].

Figures 1a and b are half-tone reproductions of cell contrast microscopic images depicting normal and OI cell cultures, respectively, in the stationary phase. This image pair is a particularly good example of how the morphology difference between normal and OI cells results in cultures with visually different textures. Although such textural differences appear to be consistent, they can be quite variable and, moreover, are often extremely subtle. For example, compare Figs. 1c and d with one another and with Figs. 1a and b.

The large variation in cell morphology makes the detection of OI by visual inspection of fibroblast culture images a nontrivial problem. A case in point is the following experiment. Two hundred twenty-four culture slides of skin fibroblast

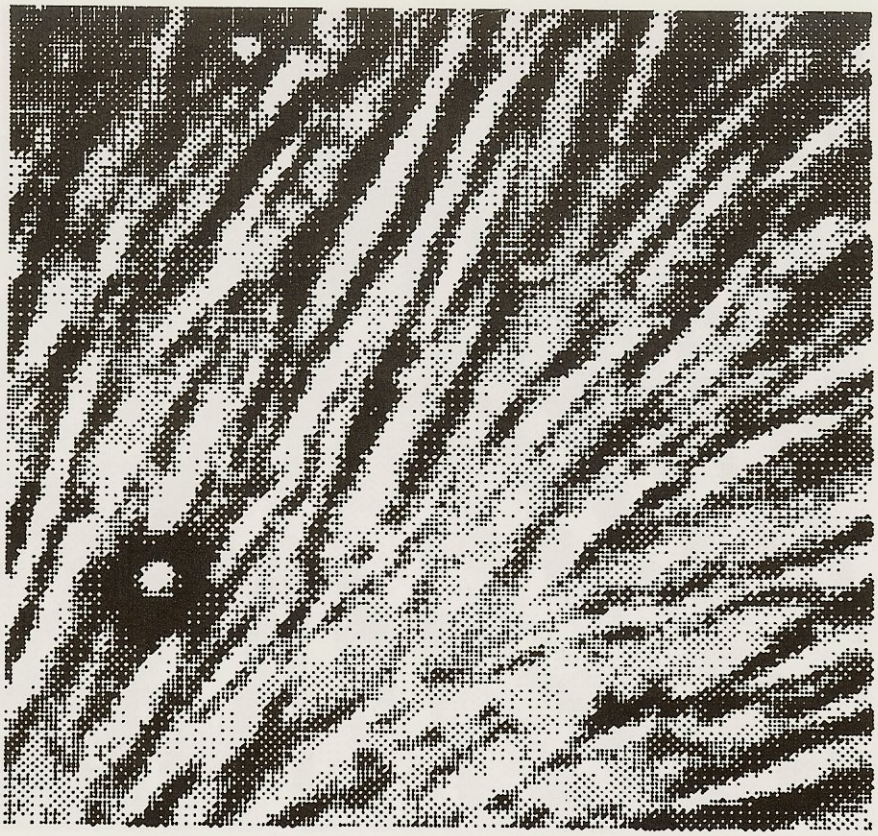

FIG. 1a. Image of a normal fibroblast culture showing the distinguishing morphological characteristics of normal cells.

cultures (in vitro), most of which were in stationary phase, were examined by a panel of six specialists at the Montreal Children's Hospital. The doctors, working independently, were instructed to classify each sample image as either normal or OI. Only 51 of the samples were unanimously placed in the same group. Of these 51 samples, only 35 were classified correctly; an accuracy of about 69%. The group of 51 samples constituted the primary data set for our computer classification experiments. Our system outperforms the specialists by a margin of about 20% on this data set.

## 3. CO-OCCURRENCE MATRICES

In this section, we formally define gray-level co-occurrence matrices (GLCMs) and generalized co-occurrence matrices (GCMs). Let $F$ be a rectangular, discrete image containing a finite number of gray levels. $F$ may be defined over the domain

$$D = \{(x, y) : x, y \in I, x \in [0, n_x), y \in [0, n_y)\},$$

by the relation

$$F = \{((x, y), k) : (x, y) \in D, k \in I, k \in [0, n_g), k = f(x, y)\},$$

FIG. 1b. Image of an OI fibroblast culture showing the distinguishing morphological characteristics of OI cells.

where $n_x$ and $n_y$ are the horizontal and vertical dimensions of $F$, $n_g$ is the number of gray levels in $F$, and $I$ is the set of integers.

The (normalized) GLCM, $G$, is a square matrix of dimension $n_g$ and is a function of both the image, $F$, and a displacement vector

$$\bar{d} = \{[x, y] : (|x|, |y|) \in D, \|[x, y]\| > 0\}$$

in the image plane, which constitutes the (second-order) spatial relation; that is,

$$G(F, \bar{d}) = \left[g_{ij}(F, \bar{d})\right].$$

Its elements, $g_{ij}$, are the probabilities of co-occurring gray levels in $F$ which are separated by $\bar{d}$:

$$g_{ij}(F, \bar{d}) = \#\{((x_1, y_1), (x_2, y_2)) : (x_1, y_1), (x_2, y_2) \in D,$$

$$[x_2, y_2] - [x_1, y_1] = \bar{d}, f(x_1, y_1) = i, f(x_2, y_2) = j\}/N,$$

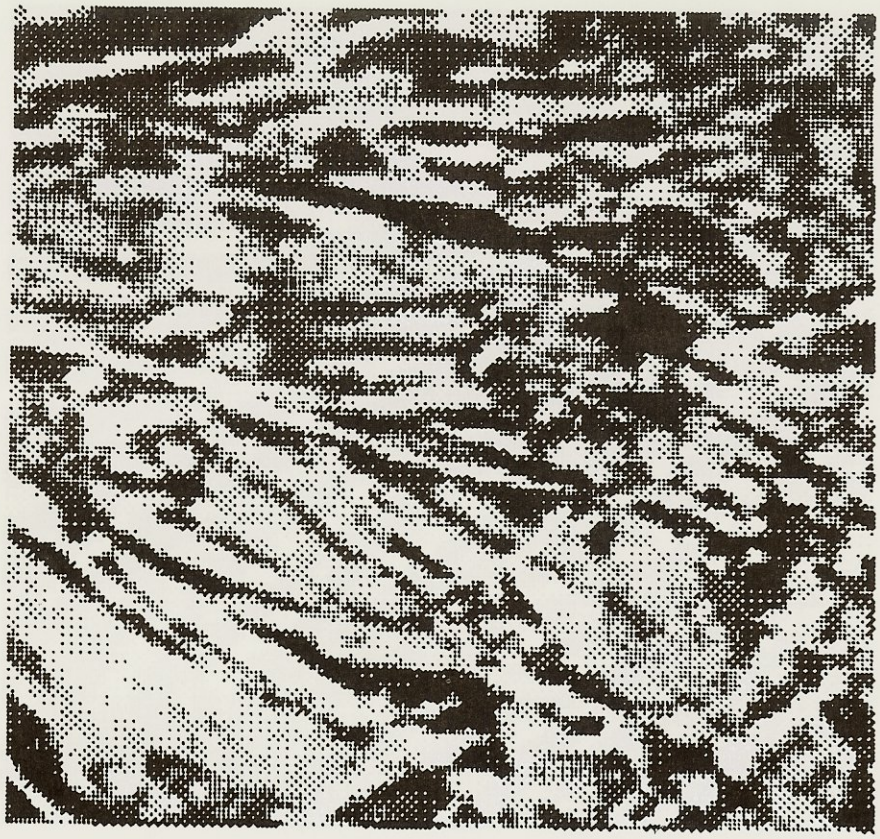

FIG. 1c. Image of a normal culture that is easily misclassified as OI.

where # denotes set cardinality. The numerator is the frequency of pairs of pixels in $F$, such that the first pixel of each pair has gray level $i$ and coincides with the tail of $\bar{d}$, while the second pixel has gray level $j$ and coincides with the head of $\bar{d}$. The denominator is a normalization factor which is equal to the total number of paired occurrences

$$N = \#\{((x_1, y_1), (x_2, y_2)) : (x_1, y_1), (x_2, y_2) \in D, [x_2, y_2] - [x_1, y_1] = \bar{d}\}$$

and serves to normalize the GLCM so that it approximates a discrete, joint probability density of co-occurring gray levels.

It is easy to show that if the direction of the displacement vector is reversed, the effect on the resulting GLCM is one of matrix transposition. Since a reversal in the direction of the displacement vector does not change the co-occurrence probabilities (GLCM elements) but simply transposes them, it does not yield any new information about the image. In practice, then, symmetric spatial relations, where no distinction is made between co-occurring pixels at the head and tail of the displacement vector, are employed. The use of symmetric spatial relations results in symmetric GLCMs. Equivalently, symmetric GLCMs may be obtained by pooling

FIG. 1d. Image of an OI culture that is easily misclassified as Normal.

frequencies of co-occurring gray levels separated by both $\bar{d}$ and $-\bar{d}$:

$$\begin{aligned} G(F, \pm\bar{d}) &= G(F, \pm\bar{d})^T \\ &= \tfrac{1}{2}\left[G(F, \bar{d}) + G(F, -\bar{d})\right] \\ &= \tfrac{1}{2}\left[G(F, \bar{d}) + G(F, \bar{d})^T\right]. \end{aligned}$$

Although there is less textural information in symmetric GLCMs than there is in asymmetric GLCMs, the former are more convenient from a computational point of view. In addition, by employing symmetric GLCMs, one effectively halves the uncomfortably large number of possible spatial relations that may have to be considered.

The GLCM was defined by specifying

1. an image feature (the pixel),
2. attributes of the feature (its position and gray level), and
3. a spatial relation (the displacement vector defined on the position attributes of pairs of features).

The definition of generalized co-occurrence matrices (GCMs) makes use of the following three generalizations.

First the notion of image feature is extended to a set of more complex features including edge points (pixels marking the location of intensity edges in the image), edge segments (formed by grouping edge points), uniform regions, etc. Let this set of features be denoted by

$$Y = \{y_i : i \in I, i \in [0, n_y)\}.$$

The second generalization allows each image feature to possess a set of attributes:

$$A = \{a_i : i \in I, i \in [0, n_a)]\}.$$

For example, an edge point can reflect the properties of the underlying image intensity profile to which it corresponds by possessing a position, a contrast, an orientation, and a fuzziness attribute. Attribute $a$ of feature $y$ can take on a number of distinct values:

$$v_a(y) = \{k : k \in I, k \in [0, n_v), v_a(y) = k\}.$$

For example, the edge point orientation attribute may be quantized to eight different integer values, in the range [0, 7], denoting angular increments of 45°.

The third generalization involves an extension of the spatial relation notion. It is convenient to define a Boolean function of pairs of features (specifically, of their position attributes),

$$R(y_i, y_j) = R'(\text{position}(y_i), \text{position}(y_j)),$$

called a spatial predicate [2]. An arbitrary second-order spatial relation between pairs of features may then be specified using an appropriate spatial predicate.

With the above generalizations, we can now define the generalized co-occurrence matrix. The GCM of an attribute, $a$, over a set of image features $Y$, pairs of which satisfy a spatial relation, $R$, is a square matrix of dimension $n_v$ and is defined as follows:

$$C(Y, a, R) = [c_{ij}(Y, a, R)],$$

where

$$c_{ij}(Y, a, R) = \#\{(y_k, y_1) : y_k, y_1 \in Y, R(y_k, y_1) = \text{TRUE}, \\ v_a(y_k) = i, v_a(y_1) = j\}/N.$$

Once again, a normalization factor

$$N = \#\{(y_k, y_1) : y_k, y_1 \in Y, R(y_k, y_1) = \text{TRUE}\}$$

is required so that the matrix will approximate a discrete joint probability density of co-occurring attributes under the given spatial relationship.

Textural information is usually extracted from co-occurrence matrices by texture descriptor functions which summarize the contents of these matrices. Fourteen such functions for GLCMs were proposed by Haralick *et al.* [5]. Four of these appear to be more useful than the rest. They are:

$$\text{(1) Angular Second Moment: ASM} = \sum_i \sum_j g_{ij}^2,$$

$$\text{(2) Contrast : CON} = \sum_i \sum_j (i-j)^2 g_{ij},$$

$$\text{(3) Entropy : ENT} = \sum_i \sum_j -g_{ij} \log g_{ij},$$

$$\text{(4) Correlation : COR} = \sum_i \sum_j (ijg_{ij} - u_x u_y)/s_x s_y,$$

where $g_{ij}$ are elements of a GLCM, $u_x$ and $s_x$ are the mean and standard deviation of the marginal probability density obtained by summing over the rows of the GLCM, and $u_y$ and $s_y$ are the corresponding statistics for the column sums. These four functions can also be used as meaningful texture descriptors for GCMs. To do this, we replace the $g_{ij}$ by $c_{ij}$, the elements of the GCM. Special care must be taken in applying the CON descriptor to GCMs, however, since the $(i-j)^2$ term must be replaced by a general dissimilarity function [2] whose form is such that it is meaningful given the particular image feature attributes used for computing the GCM. For example, the appropriate dissimilarity function for edge point orientations quantized to $n$ values, equally spaced in the range $[0, 2\pi]$, is

$$\text{dis}(i, j) = \left| \sin\left( \frac{\pi}{2(n-1)} (i-j) \right) \right|.$$

The interpretation of these descriptors in terms of various perceived properties of texture are discussed in [5] and [2].

The success of co-occurrence-based representations in applications, especially those involving the use of pattern recognition techniques for texture discrimination, is often critically dependent on the fidelity with which the co-occurrence matrices capture the structure of the underlying textures. This, in turn, is dependent on the particular spatial relations used for computing the co-occurrence matrices. In previous research, we formulated a statistical approach for finding those spatial relations which yield matrices that maximally capture a texture's structure [12]. These matrices are the ones to be preferred for the design of successful pattern classifiers.

Assuming that a texture is structured (i.e., that it is generated by a process that is not purely random), then a GLCM that captures this structure should have highly dependent rows and columns. That is, pixel gray levels occurring at one end of the displacement vector should bias the probabilities of gray levels occurring at the other end. This assumption is reasonable, to a greater or lesser extent, for many natural textures. It motivates a quantitative (chi-square) measure of the row/column independence of co-occurrence matrices. It is important to have a measure of this sort available because it represents a means of finding those spatial relations which yield optimally performing matrices. One of the results of experiments involving this

measure is that the best performing co-occurrence matrices are those that are computed using displacement vectors whose lengths are equal to the size of the textural primitives [12]. This result is exploited in our OI detection system, which is described next.

## 4. IMPLEMENTATION AND RESULTS

To discriminate images of normal fibroblast cultures from OI cultures, we employ standard pattern recognition techniques [3]. A number of texture descriptors are derived from GLCMs and GCMs, computed over a culture image. These descriptors constitute a feature vector (of length $L$) which describes the texture depicted in the image. Each image thus represents a sample point in ($L$-dimensional) feature space. The classification problem is to find separating hypersurfaces, or decision boundaries, which partition feature space into a number of hypervolumes designating different classes. A simple way of determining the decision boundaries is by a "supervised

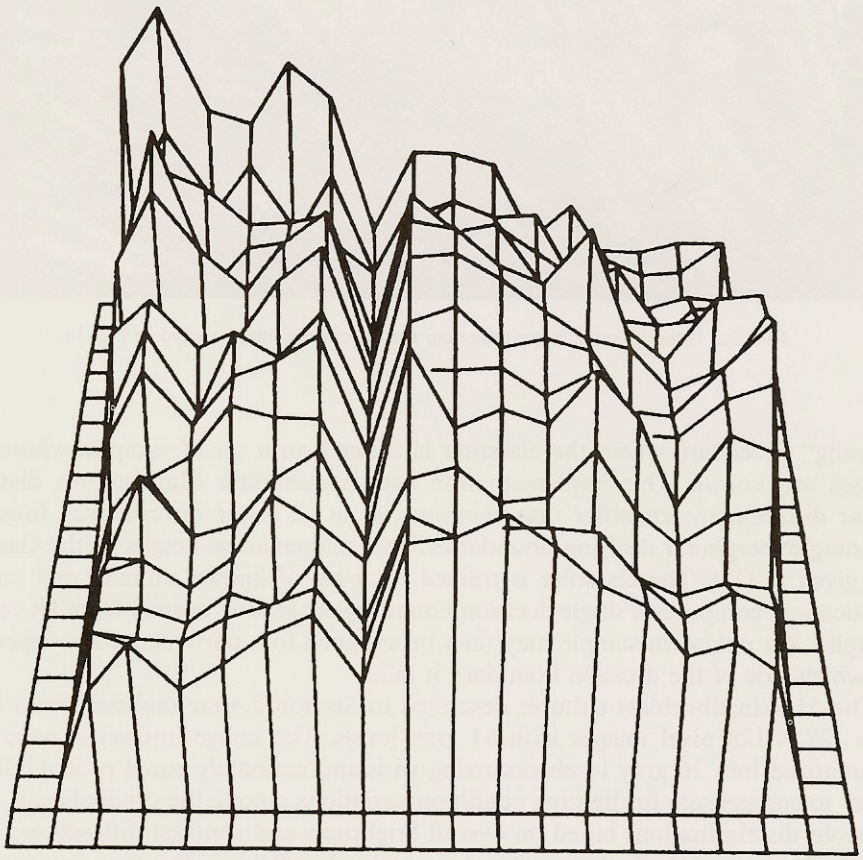

FIG. 2. Gray-level co-occurrence matrix (dimensions $16 \times 16$) computed over the texture of Fig. 1a using displacement vector $[-8, 8]$. (Note that the matrix is shown as a surface in 3-space, under perspective projection. Matrix elements form a grid of points whose heights above the base plane correspond to the scaled magnitude of these elements. The main diagonal of the matrix runs from the upper left to the lower right corner of the plane.

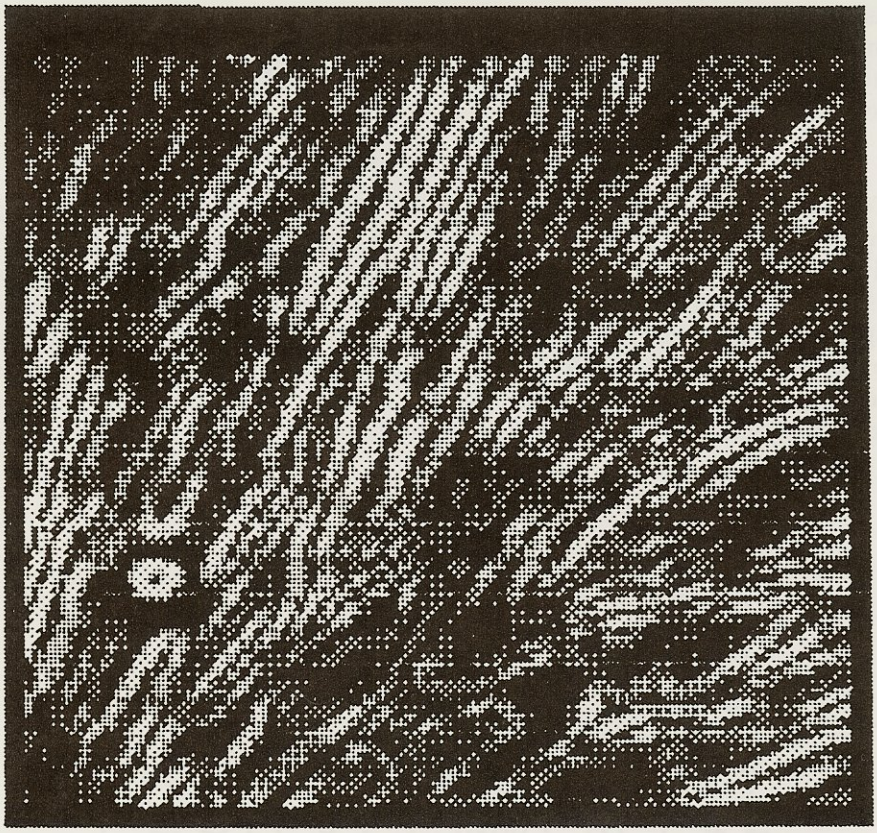

FIG. 3a. Intensity edge magnitude map for the culture image shown in Fig. 1a.

training" procedure where the classifier is trained on a set of samples whose true classes are known. Our implementation uses a minimum Mahalanobis distance, linear discriminant classifier that computes a set of linear discriminant functions defining hyperplanar decision boundaries. The mathematical details of the classifier are given in [12]. The classifier is trained on a set of known samples and, in this application, computes a single decision boundary separating normal from OI culture samples. An unknown sample may then be assigned to a particular class depending on which side of the decision boundary it falls.

The 51 skin fibroblast cultures described in Section 2 were digitized from slides into $128 \times 128$ pixel images with 64 gray levels. The image intensities were then requantized into 16 gray levels occurring with approximately equal probabilities in order to compensate for lighting condition variations among the originals and, thus, to avoid discriminations based on overall brightness and contrast differences.

The elements of the feature vectors are obtained as follows. The first set of texture descriptors are derived from symmetric GLCMs, computed using spatial displacement vectors aligned along four directions, $\bar{d} \in \{[k, 0], [k, k], [0, k], [-k, k]\}$. The size of the displacement vectors, $k$, was chosen to be eight pixels so that it matches the average size of the textural primitives which, for these textures, are individual

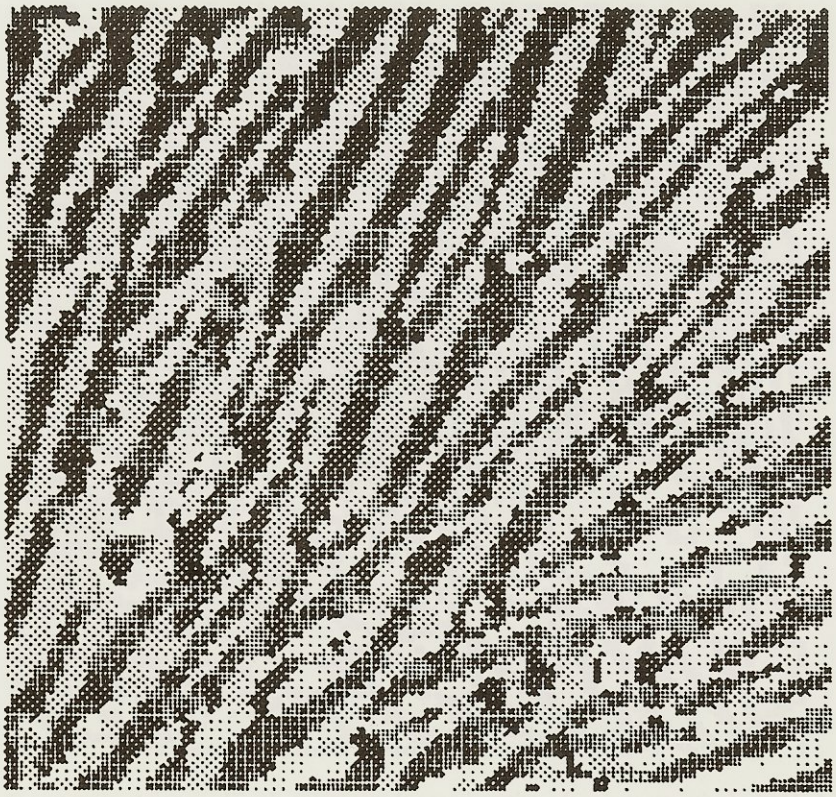

FIG. 3b. Intensity edge orientation map for the culture image shown in Fig. 1a. Note that the directions are quantized to eight values in 45° increments.

fibroblasts. The reasons for using this criterion in selecting $k$ were outlined at the end of the previous section. A GLCM obtained from the cell culture image of Fig. 1a is shown in Fig. 2. The ASM, CON, ENT, and COR texture descriptors are then computed over the four matrices obtained using the chosen value of $k$. The first eight elements of each feature vector are the means and ranges of these four descriptors.

More information about the shapes of cells is obtained from the next set of texture descriptors, which are derived from GCMs based on directions of edge point image features. The edge point features are obtained as follows. A $5 \times 5$ edge operator (described in the Appendix) is first convolved with the image. The operator generates an edge magnitude and edge orientation (quantized to eight values representing 45° increments) at each point in the image. Figure 3a is the edge magnitude map and Fig. 3b is the edge orientation map for the image in Fig. 1a. The magnitude response is then thresholded and the marked edge regions are thinned. The thinning is accomplished by supressing any marked pixel, if there exist other such pixels having higher magnitudes and lying on a line perpendicular to the marked pixel's orientation. This line extends for a length of 2 pixels on either side of the marked pixel. The remaining edge points are the set of local features and have position and orientation attributes. Figure 4 shows the edge point features for the

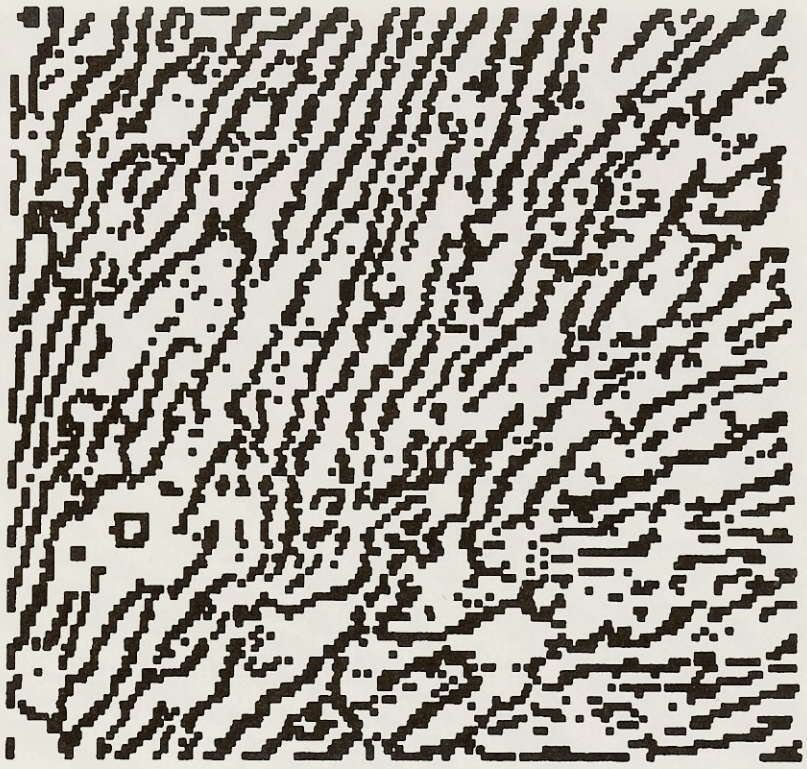

FIG. 4. Marked edge points for the culture image shown in Fig. 1a. These points constitute the set of features on which the generalized co-occurrence matrices are built.

image in Fig 1a. Note how the predominant borders of individual cells have been extracted. The spatial predicate, used for computing the GCM over edge point orientations, is TRUE if the (city block) distance between two edge pixels is less than or equal to $k/2$, where $k$ is the distance determined above. A GCM resulting from the image in Fig. 1a is shown in Fig. 5. Finally, the remaining four elements of the feature vector are the values of the ASM, CON, ENT, and COR texture descriptors computed over this GCM.

The classifier was trained on the 51 feature vectors and the training set was then reclassified as either normal or abnormal. The results are as follows. Approximately 90% of the images were correctly classified. Confusion tables for the computer and expert's classification are shown in Fig. 6. In addition to the better overall performance, the system is more conservative than the experts. That is, it tends to diagnose more cultures as OI than the experts do.

Preliminary experiments had shown that, for this problem, the GLCM descriptors alone or the GCM descriptors alone, perform about equally, and at a level which is approximately 13% lower than the set of combined descriptors (see Fig. 7). This extra 13% comes from the combined use of edge and intensity information. For a more detailed discussion, and for a comparison of our method with other approaches to texture classification, see [10].

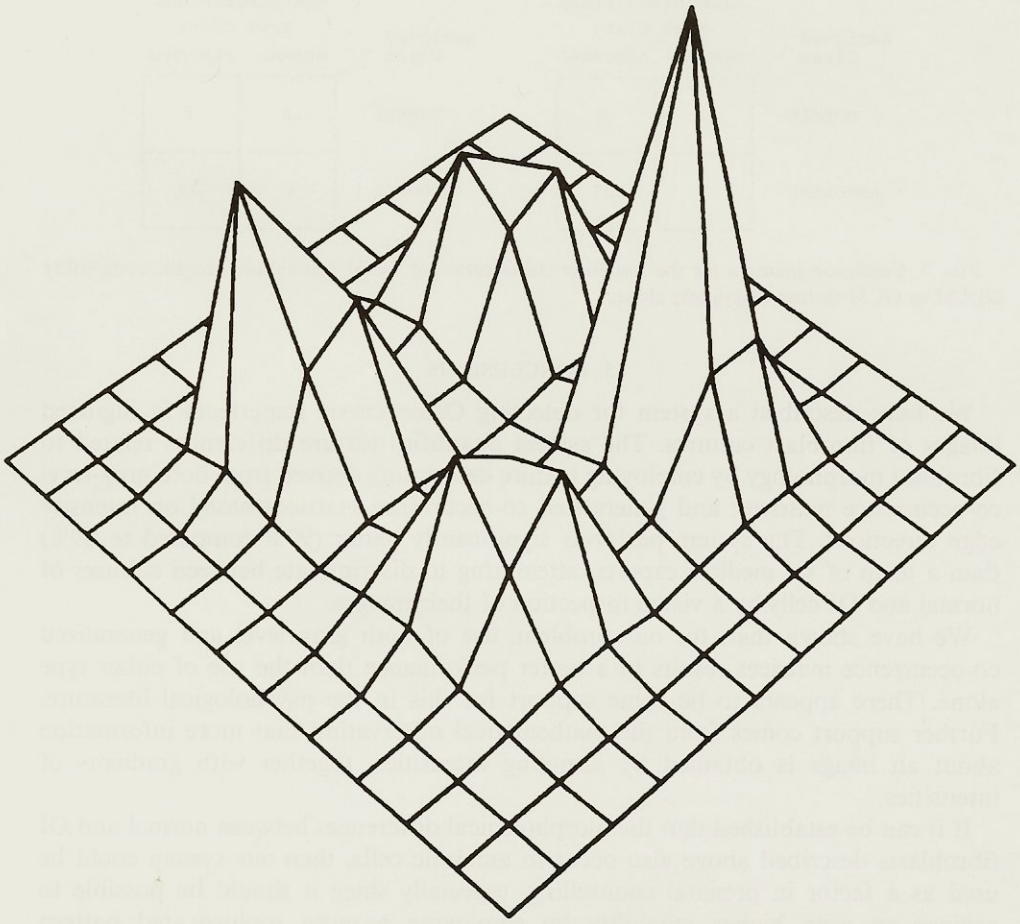

FIG. 5. Edge direction GCM (dimension 8 × 8) computed over the set of features shown in Fig.4. Note that the main diagonal of the matrix runs from the left to the right corner. The prominant peaks, centered at grid points corresponding to co-occurring edge directions of 1–1, 5–5, 1–5, and 5–1, indicate that the cells in the culture shown in Fig. 1a have major axes oriented predominantly at 45° with respect to the horizontal. Furthermore, the deep valleys indicate that very few cell borders run in perpendicular directions. The low variance of cell orientations indicates that this culture is likely to be normal.

COMPUTER CLASSIFICATION

| Assigned Class \ True Class | NORMAL | ABNORMAL |
|---|---|---|
| NORMAL | 11 | 3 |
| ABNORMAL | 2 | 35 |

EXPERT'S CLASSIFICATION

| Assigned Class \ True Class | NORMAL | ABNORMAL |
|---|---|---|
| NORMAL | 12 | 15 |
| ABNORMAL | 1 | 23 |

FIG. 6. Confusion matrices for the computer and expert's classification performances for the 51 cell culture images.

GLCM DESCRIPTORS

| Assigned Class \ True Class | NORMAL | ABNORMAL |
|---|---|---|
| NORMAL | 11 | 8 |
| ABNORMAL | 3 | 29 |

GCM DESCRIPTORS

| Assigned Class \ True Class | NORMAL | ABNORMAL |
|---|---|---|
| NORMAL | 10 | 8 |
| ABNORMAL | 4 | 29 |

FIG. 7. Confusion matrices for the computer classification of the 51 cell culture images, using either GLCM or GCM texture descriptors alone.

## 5. CONCLUSIONS

We have described a system for detecting Osteogenesis Imperfecta in digitized images of fibroblast cultures. The system quantifies texture differences related to fibroblast morphology by employing texture descriptors derived from both gray-level co-occurrence matrices, and generalized co-occurrence matrices based on intensity edge directions. The system performs significantly better (90% compared to 69%) than a team of six medical experts, attempting to discriminate between cultures of normal and OI cells by a visual inspection of their images.

We have shown that, for our problem, use of both gray level and generalized co-occurrence matrices results in a better performance than the use of either type alone. There appears to be some support for this in the psychological literature. Further support comes from the mathematical observation that more information about an image is obtained by sampling intensities, together with gradients of intensities.

If it can be established that the morphological differences between normal and OI fibroblasts described above also occur in amniotic cells, then our system could be used as a factor in prenatal counselling, especially since it should be possible to achieve an even higher reliability by employing a more sophisticated pattern classifier.

## APPENDIX: AN EDGE OPERATOR

The edge operator which was used in the OI detection system is a variation of the operator suggested by Kirsch [1971] as it was used by Davis *et al.* [1979]. The operator requires a partition of the $5 \times 5$ neighbourhood of a point, $p = (x, y)$, in the image into the eight regions, $r0, \ldots, r7$ shown below.

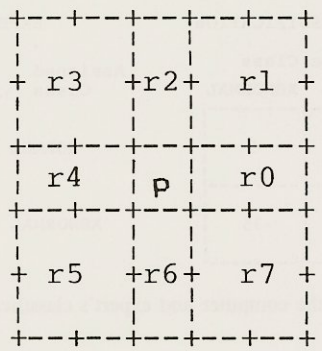

However, our operator assigns edge magnitudes and orientations differently from that of Davis *et al.* Let

$$a_i = \max\left[0, 5\left(\sum_{j=0}^{2} rk\right) - 3\left(\sum_{j=3}^{7} rk\right)\right],$$
$$i = 0, 1, \ldots 7, \qquad k = i + j \bmod 8. \tag{1}$$

Then, the edge magnitude at $p$ is given by

$$M(p) = \max_{i=0}^{7} a_i$$

and the edge orientation is

$$O(p) = L(\pi/4),$$

where $L$ is equal to the value of $i$ which maximizes $M$. By convention, the orientation is assigned so that, when facing in the direction of the edge, the brighter side is on the left.

Our operator gives a much more homogeneous orientation response than the operator suggested by Davis *et al.* The notable difference is in (1), where a max function is used instead of the absolute value function used by Davis. The max function suppresses large negative values of its argument which would otherwise lead to many spuriously assigned orientations near intensity edges in the image. The resulting orientation response is more consistent, a property that is particularly important for the computation of edge orientation based co-occurrence matrices in the OI detection application.

## REFERENCES


1. T. Caelli and B. Julesz, On perceptual analyzers underlying visual texture discrimination, I, II, *Biol. Cybernet.* **28**, 1978, 167–175, and **29**, 1978, 201–214.
2. L.S. Davis, S. Johns, and J. K. Aggarwal, Texture analysis using generalized co-occurrence matrices, *IEEE Trans. Pattern Anal. Mach. Intell.* **3**, 1979, 251–259.
3. R. O. Duda, and P. E. Hart, *Pattern Classification and Scene Analysis*, Wiley, New York, 1973.
4. R. M. Haralick, Statistical and structural approaches to texture, *Proc. IEEE*, **65**, 1979, 786–804.
5. R. N. Haralick, K. Shanmugam, and I. Dinstein, Textural features for image classification, *IEEE Trans. Systems Man Cybernet.* **11**, 1973, 610–621.
6. B. Julesz, Visual pattern discrimination, *IRE Trans. Inform. Theory* **1**, 1962, 84–92.
7. G. Lancaster, H. Goldman, C. R. Scriver, R. J. M. Gold, and I. Wong, Dominantly inherited Osteogenesis Imperfecta in man: An examination of collagen biosynthesis, *Pediatrics Res.* **9**, 1975, 83–88.
8. D. Marr, Early processing of visual information, *Phil. Trans. Roy. Soc. London Ser. B* **275**, 1976, 483–534.
9. V. A. McKusick, *Heritable Disorders of Connective Tissue*, 4th ed., C. V. Mosby Co., St. Louis, 1972.
10. D. Terzopoulos, *Applying Co-occurrence Matrices to Texture Analysis*, M. ENG THESIS, Dept. of Electrical Engineering, McGill University, April, 980.
11. J. Weszka, C. Dyer, and A. Rosenfeld, A comparative study of texture measures for terrain classification, *IEEE Trans. Systems Man Cybernet.* **4**, 1976, 269–285.
12. S. W. Zucker, and D. Terzopoulos, Finding structure in co-occurrence matrices for texture analysis, *Computer Graphics and Image Processing* **12**, 1980, 286–308.
13. Kirsch, R. A., Computer identification of the constituent structure of biological images, *Comput. Biomed. Res.* **4** 1971, 315–328.